Perturbation of Turbulent Boundary Layer by Outer Layer and Inner Layer Devices for Turbulent Noise Source Reduction

Chioma Muhammad* and Tze Pei Chong†
Brunel University London, Uxbridge, UB8 3PH, UK

An application of the Large Eddy BreakUp (LEBU) as a source-targeting device to mitigate the wall pressure fluctuations and lateral coherence length scale of a turbulent boundary layer is investigated. Both represent the prominent noise sources for the trailing edge noise radiation. When a LEBU is placed strategically at the outer part of a turbulent boundary layer, the wall pressure spectra can establish a self-similar behaviour against s', which is a normalised separation distance between the LEBU's trailing edge and the targeted location for noise mitigation. It is found that s' has to be greater than 3 in order to achieve an overall reduction in the wall pressure fluctuations. However, this criterion does not apply to the lateral coherence length. The combined effect would reduce the effectiveness of the LEBU to abate the frequency-integrated, overall noise radiation. Under the principle of non-interference, a joint-implementation of RIblets and LEBU (RIBU) can produce promising results where reduction of the frequency-integrated, overall noise radiation can be achieved, again at $s' > 3$.

I. Introduction

One of the major noise sources for an aerofoil is the trailing edge self-noise [1]. When the boundary layer has undergone a complete transition to fully turbulent at the trailing edge, a cascade of turbulent length scale eddies are scattered into a broad frequency band of acoustic disturbances into the far field.

An effective strategy for the mitigation of the radiated turbulent broadband noise is to execute the *source targeting* through manipulation, altering or inhibiting the growth mechanisms of the turbulent boundary layer. More specifically, efforts to execute the source targeting can focus on either the inner part, or the outer part of a turbulent boundary layer, respectively. Recently, we disseminated some results on the use of riblets to target the inner part of turbulent boundary layer for the mitigation of turbulent noise sources on a flat plate system [2]. Although no acoustic results are available, the near-wall turbulence structures are found to dissipate quite rapidly when crossing the riblets surface. The riblets can slightly reduce the wall fluctuating pressure power spectral density level at the low and high frequency ranges, but cause an increase at the mid frequency range. On the other hand, the lateral turbulence coherence length scale across a large frequency range can be reduced by the riblets. The combined effects give rise to an effective mitigation of the turbulent noise source at the low and high frequency regions by the riblets, potentially transferable to the trailing edge noise reduction.

A classical outer layer manipulator is the Large Eddy Break Up (LEBU) device, which consist of a two-dimensional thin plate or aerofoil placed onto the outer part of a turbulent boundary layer. They are placed in such a way that the wake emanated from the LEBU can disrupt the turbulence structure self-sustaining mechanisms of momentum transport into the boundary layer downstream. The aim is to target large turbulent eddies in the boundary layer, and break them up into smaller, lower energy eddies that will eventually dissipated by the viscosity [3]. Studies have also been conducted by [4] using a number of horizontal plates suspended over the flow surface so that there is interaction with the outer layer of the boundary layer. They observe a 24% reduction of skin friction over a longitudinal range of 45 device heights, although a net drag reduction cannot be realised presumably due to the increased parasite drag incurred by the supporting struts of the LEBU. When derived from their velocity fluctuating spectra, [5] describe the penetration of small scale eddies to the boundary layer via the wake of the LEBU, which also acts as a shield to prevent incursions of high speed fluid from the outer layer to the near wall region.

The previous works on the LEBU as an outer layer device for turbulent drag reduction suggest that it has a potential to execute an effective source targeting to achieve turbulent self-noise reduction. This paper will investigate the potential of LEBU for the reduction of turbulent wall pressure sources that are important for aerofoil self-noise radiation. To the best knowledge of the authors, the change in the turbulence structures by LEBU has not been studied much from the

*Research Engineer, Dyson, Chioma.Muhammad@gmail.com, Non-AIAA Member.
†Reader, Department of Mechanical and Aerospace Engineering, t.p.chong@brunel.ac.uk, AIAA Member.

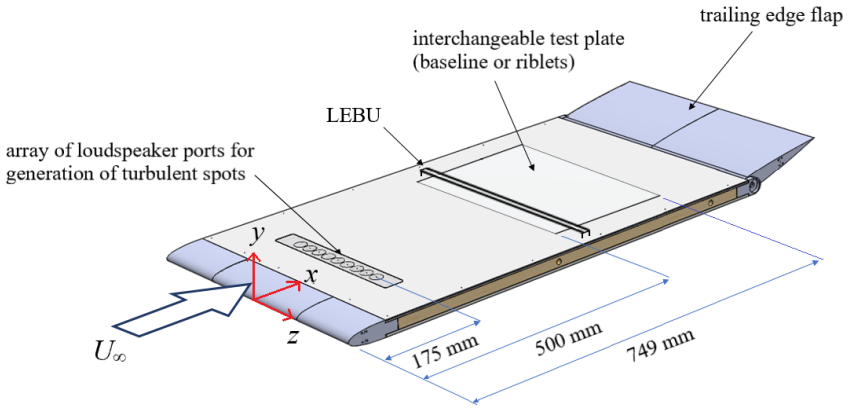

Fig. 1 Schematic showing the flat plate model used in the current study. The coordinate system is also shown. Drawing is not to scale.

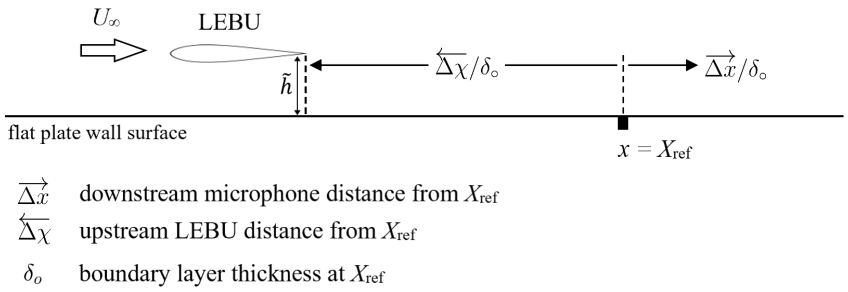

Fig. 2 Schematic showing the LEBU arrangement. Drawing is not to scale.

perspectives of the wall pressure fluctuation field. Furthermore, it still remains relatively scarce in the literature that describes the turbulence spectral characteristics produced by LEBU, including the manipulation for the turbulence lateral coherence length scale. This paper aims to shed some lights on LEBU for their potential to be a trailing edge self-noise reduction device. This paper will also explore a combination of RIblets and LEBU, i.e. which can be abbreviated as the RIBU, for their effectiveness to enhance the source targeting to mitigate turbulent noise sources.

II. Experimental Setup

The experiments were conducted in an open circuit, suction type wind tunnel where the axial fan is driven by a 7.5 kW motor capable of achieving velocity up to 35 $\mathrm{m\,s^{-1}}$ inside the 0.5×0.5 m working section. The walls are constructed by Perspex to allow optical access. The mean turbulence intensity of the flow is measured to be less than 0.5%.

A. Design of a flat plate system with LEBU

The flat plate system developed in [2], which has a semi-hollow section to allow the interchange between a baseline (smooth surface) test plate and a riblets test plate, is employed here for the study of LEBU. As shown in Figure 1, a flat plate that contains a recess in the middle section for interchangeable test plates was designed and built in-house. The coordinate system used in this study is also shown in the figure, where *x, y* and *z* denote the streamwise, wall-normal and lateral directions, respectively. In the figure, $x = 0$ refers to the leading edge of the flat plate. When a fully developed two-dimensional turbulent boundary layer is required, a zig-zag type turbulator will be placed at the same location as the loudspeaker strip, $x = 175$ mm, to serve as a passive device to artificially trip the boundary layer into turbulent. Note that the loudspeaker strip is used as an active triggering device to generate the turbulent spots. Results pertaining to the turbulent spots are not included in the present paper.

$\overleftarrow{\Delta\chi}$ (mm)	5	15	30	50	80
$\overleftarrow{\Delta\chi}/\delta_\circ$ at 10 m s^{-1}	0.440	1.321	2.643	4.405	7.047
$\overleftarrow{\Delta\chi}/\delta_\circ$ at 12 m s^{-1}	0.461	1.382	2.763	4.605	7.369
$\overleftarrow{\Delta\chi}/\delta_\circ$ at 15 m s^{-1}	0.476	1.428	2.856	4.761	7.617

Table 1 Dimensional ($\overleftarrow{\Delta\chi}$) and non-dimensional ($\overleftarrow{\Delta\chi}/\delta_\circ$) distances of the LEBU's trailing edge placement in the upstream direction from $X_{\mathbf{ref}}$.

$\overrightarrow{\Delta x}$ (mm)	0 (X_{ref})	20	40
$\overrightarrow{\Delta x}/\delta_\circ$ at 10 m s^{-1}	0	1.762	3.524
$\overrightarrow{\Delta x}/\delta_\circ$ at 12 m s^{-1}	0	1.842	3.684
$\overrightarrow{\Delta x}/\delta_\circ$ at 15 m s^{-1}	0	1.904	3.808

Table 2 Dimensional ($\overrightarrow{\Delta x}$) and non-dimensional ($\overrightarrow{\Delta x}/\delta_\circ$) distances of the measurement locations in the downstream direction from $X_{\mathbf{ref}}$.

An illustration of the LEBU system is shown in Figure 2. The LEBU is a NACA0014 symmetrical aerofoil with chord length C_{LEBU} = 15 mm, which entails a maximum thickness of approximately 2 mm to resemble a thin structure, and yet remain a sturdy device. The LEBU is supported by struts that are laser-cut from 0.5 mm thick plywood. Two heights of struts have been used in this study, which will raise the centreline and trailing edge of the LEBU to a height of $\tilde{h}$ = 2.5 mm and 5.0 mm above the surface of the flat plate, henceforth referred to the LEBU$_{2.5}$ and LEBU$_{5.0}$, respectively. The struts carrying the entire LEBU are movable in the streamwise direction, which will be described by a non-dimensional distance of $\overleftarrow{\Delta\chi}/\delta_\circ$ as depicted in Figure 2. With the designation that the main flow is from left to right, the overhead left arrow in $\overleftarrow{\Delta\chi}$ emphasises the direction of which the LEBU is moved upstream from a reference location, X_{ref}, where $X_{\mathrm{ref}} = x = 625$ mm. $\delta_\circ$ is the boundary layer thickness measured at X_{ref}. As a summary, $\overleftarrow{\Delta\chi}/\delta_\circ$ is a non-dimensional distance between X_{ref} and the LEBU's trailing edge. In this study, there are total of five $\overleftarrow{\Delta\chi}$ locations tested under three freestream velocities U_∞ = 10, 12 and 15 m s^{-1}. The tabulated values can be found in Table 1.

For the test plate system, there is a recess between $500 \leq x \leq 749$ mm to house either a baseline, smooth surface test plate, or riblets surface test plate. Both test plates have the same overall length. For the baseline test plate, it has a smooth aluminium finish enabled by a 3-axis CNC machining. The plate consists of arrays of streamwise and lateral distributed pressure tap holes of 0.4 mm diameter for the measurement of the wall pressure fluctuations. The streamwise locations of these pressure taps are x = 625 (X_{ref}), 627, 634, 645, 655, 665, 685 and 725 mm, all of whom will be used simultaneously to measure the convection rates of the turbulent eddies. In the discussion of the wall pressure spectra results, however, only three streamwise locations (x = 625 (X_{ref}), 645, and 665 mm) will be considered. They are expressed as $\overrightarrow{\Delta x}$ = 0, 20 and 40 mm, respectively, where the overhead right arrow emphasises the direction of which the measurement location is moved downstream from X_{ref} as depicted in Figure 2. In what follows, they will be non-dimensionalised by the boundary layer thickness measured at the reference location, which give rise to $\overrightarrow{\Delta x}/\delta_\circ$ as summarised in Table 2.

Combining the LEBU placements in Table 1 with the targeted locations for noise mitigation in Table 2 will give rise to 45 unique combinations of $s' = (\overleftarrow{\Delta\chi}/\delta_\circ + \overrightarrow{\Delta x}/\delta_\circ)$. s' is therefore a non-dimensional separation distance between the LEBU's trailing edge and the targeted location for noise mitigation.

The flat plate also contains multiple pressure taps in the lateral direction to measure the lateral coherence length of the turbulence. This particular lateral array is situated at $x = X_{\mathrm{ref}}$, where the lateral spacing is Δz = 2.0, 4.2, 6.6, 9.2, 12.0, 15.0 and 18.2 mm from the central of the test plate.

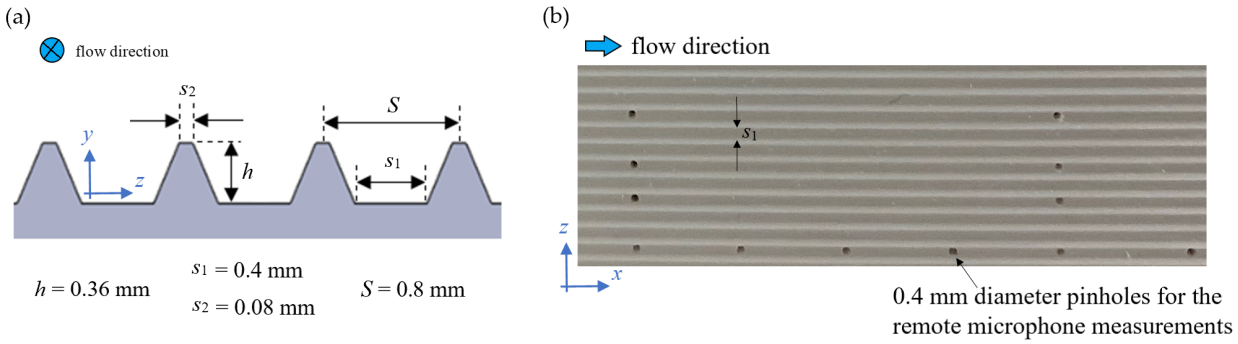

Fig. 3 (a) Schematic (front view) illustrating the riblets geometry, and (b) photograph (plan view) showing a zoomed-in view (~ 29.0 mm × 9.2 mm) of the riblets test plate used in the current study.

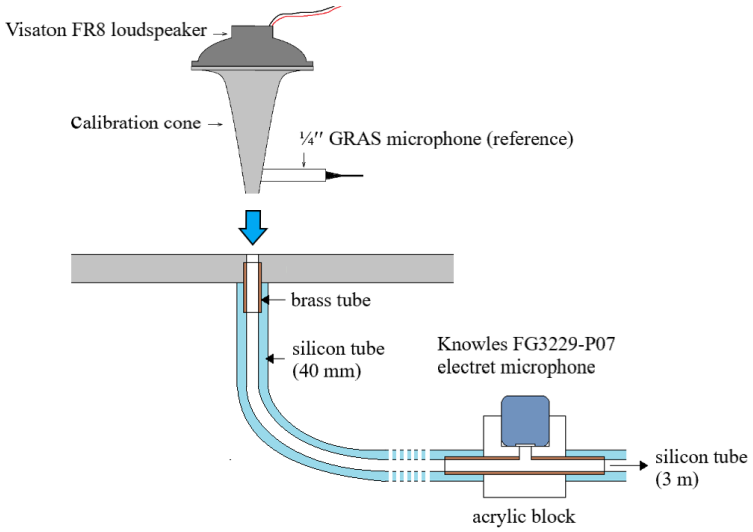

Fig. 4 The remote microphone configuration (cross section view), including the calibration system.

B. Design of the riblets plate

In the experiments when only the LEBU is utilised, the flat plate is of the smooth surface type. The flat plate will only be replaced to the riblets type when the "RIBU" configuration is investigated. The riblets test plate is manufactured in-house by a Stereolithography Apparatus (SLA) 3D printing technique. Figure 3 summarises the riblets configuration and dimensions. Note that the spanwise distribution of the pressures tab for the riblets plate can be slightly different compared to the values of the smooth flat plate. This is due to the adjustment of the pressure tab to ensure that it is located within the valley of each groove of the riblets. Nevertheless, the difference is very small (≤ 0.3 mm), thus can be treated as negligible. More information about the design process of the riblets plate can be found in [2].

C. Instrumentation

The Knowles FG3229-P07 electret microphones, which are circular (2.57 mm diameter) with a sensing diameter of 0.8 mm, have been used in the wall pressure fluctuation measurements. As shown in Figure 4, the microphone is mounted remotely underneath the wall surface with an acrylic holder. It is connected to the wall surface via a 40 mm silicone tube. The same type of silicone tube of about 3 m long is connected to the other end of the acrylic holder, which will come out from the working section of the wind tunnel. The use of a long tube at the other end is to ensure that the acoustic waves travelling inside the remote microphone system does not encounter a sudden termination that will result in the backward reflection.

A Visaton FR8 10W full range speaker is used to calibrate each of the remote microphone *in-situ*. It is attached to a

cone that is designed to direct the sound pressure waves from a larger area to the other end of a smaller area. A similar calibration method was used by both [6] and [7]. In this method, a $\frac{1}{4}''$ GRAS reference microphone with a known frequency response is embedded in the wall of the cone near the surface as shown in Figure 4. This allows the signal of the remote microphone and reference microphone to be measured simultaneously, thereby allowing us to determine the phase function of each remote microphone. During the experiment, the raw data from each remote microphone is sampled at a rate of 40 kHz for 15 seconds, which amounts to 600,000 samples. The data acquisition system has a 16-bit resolution and each sampling channel has a built-in anti-aliasing filter.

The flow velocity fluctuation is measured by a miniature, single hot wire (Dantec 55P11), which consists a 1.25 mm long, 5 μm diameter tungsten sensing wire. Operated by a constant temperature anemometer, the overheat ratio of the hot wire is set to 1.8, which will facilitate an operating temperature of the hot wire to be approximately 300°C. The hot wire is attached to a three axis traverse system, in which the step motors are capable of achieving very fine movement of 0.01 mm. Such a high spatial resolution in the traverse is suitable for the boundary layer measurement. The analogue-to-digital (A/D) card used in the hot wire acquisition has an 12-bit resolution. The data sampling rate is set at 20 kHz for 13 seconds. A low-pass filter of 10 kHz is utilised in the data acquisition to ensure that the sampled signal is inside the Nyquist frequency and is not contaminated by aliasing. Temperature correction of the sampled hot wire signals is performed during the post-analysis.

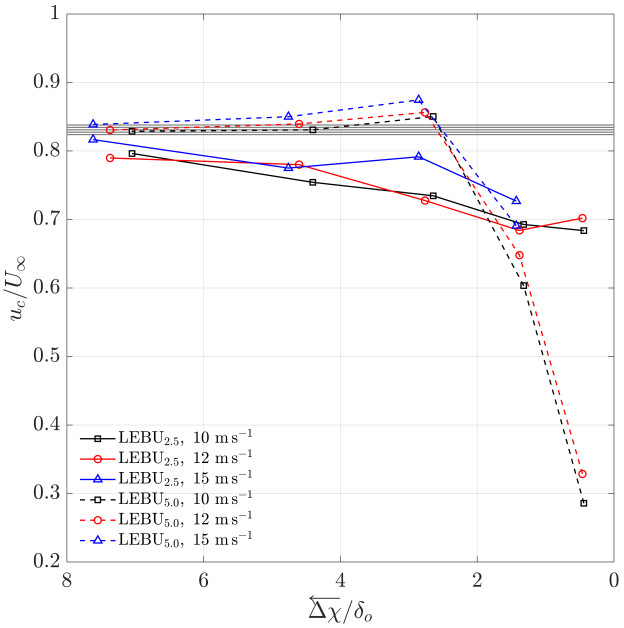

Fig. 5 Convection velocities of the turbulence eddies as a function of $\overleftarrow{\Delta\chi}/\delta_\circ$ at U_∞ = 10, 12 and 15 m s^{-1} by the LEBU. The datum range produced by the baseline flat plate is indicated by the horizontal multiple lines.

III. Results

The results presented here can provide a basis for the outer layer device in the form of LEBU to reduce aerofoil trailing edge self-noise. The measurement campaign includes experiments conducted at three freestream velocities, U_∞ = 10, 12 and 15 m s^{-1}, which serve to facilitate a sensitivity study for the spatial distributions of LEBU ($\tilde{h}$ and $\overleftarrow{\Delta\chi}/\delta_\circ$) and their effect to the wall pressure turbulent noise sources production.

A. Turbulence wall pressure convection

A cross-correlation in the spatial-temporal domain for the longitudinal wall pressure fluctuations is conducted. The output of this analysis is the cross-correlation coefficient $R_{x_i x_j}$ as a function of time delay between signals, τ, which can be used to determine the convection velocity of the most prevalent scale of turbulence structures. In the present experiments, all the streamwise cross-correlation studies were conducted by taking reference to the most upstream

microphone sensor at $x = X_{\text{ref}} = 625$ mm. The convection time for the most dominant wall pressure generating structures to traverse between them can be identified by the $\tau_{\max}$ corresponding to the maximum cross-correlation coefficient $R_{x_i x_j \max}$. From a dataset of $(\overrightarrow{\Delta x}, \tau_{\max})$, an average convection velocity of the dominant turbulent eddies can be determined. It should be noted that the most dominant turbulent eddies in the boundary layer would decay at a slower rate than the small-scale turbulent eddies.

Figure 5 shows the normalised convection velocities of the turbulence eddies u_c/U_∞, as a function of $\overleftarrow{\Delta\chi}/\delta_\circ$, at $U_\infty = 10$, 12 and 15 m s^{-1}, where U_∞ is the freestream velocity. As a reminder, $\overleftarrow{\Delta\chi}$ represents the upstream distance from X_{ref} (see Figure 2), where $\delta_\circ$ is the boundary layer thickness measured at X_{ref}. The figure demonstrates that the LEBU can slow down the longitudinal turbulence convection considerably for both the $\text{LEBU}_{2.5}$ and $\text{LEBU}_{5.0}$ types, but will slowly recover to the baseline datum as the $\overleftarrow{\Delta\chi}/\delta_\circ$ increases. The deviation from the baseline datum is the most significant at low $\overleftarrow{\Delta\chi}/\delta_\circ$, i.e. when the LEBU is at the closest proximity to X_{ref}. This illustrates that the velocity deficit of the near wake emanated from the LEBU can exert a retarding impact to cause a slow down of the local turbulence convection. The reduction in turbulence convection is the most pronounced for the $\text{LEBU}_{5.0}$ case, where a reduction to $u_c/U_\infty \approx 0.3$ is observed. However, what appears to be a significant reduction in turbulence convection initially is followed by a steep recovery and return to the baseline datum as $\overleftarrow{\Delta\chi}/\delta_\circ$ continues to increase, i.e. the LEBU moves further upstream and away from X_{ref}. It is also worth noting that in almost all cases an overshoot in the turbulence convection appears at $2.5 \leq \overleftarrow{\Delta\chi}/\delta_\circ \leq 4.5$, before returning to the baseline level at $\overleftarrow{\Delta\chi}/\delta_\circ > 5$.

However, a very different response of the turbulence convection is produced when the LEBU is lowered to $\tilde{h} = 2.5$ mm ($\text{LEBU}_{2.5}$). While it still exhibits a reduction when the LEBU is situated near the X_{ref}, the u_c/U_∞ will recover almost in a linear fashion as $\overleftarrow{\Delta\chi}/\delta_\circ$ increases. However, the recovery is slower, and does not quite reach the baseline datum within the range of $\overleftarrow{\Delta\chi}/\delta_\circ$ investigated here.

Figure 5 provides a clear indication that both the $\text{LEBU}_{2.5}$ and $\text{LEBU}_{5.0}$ are capable of disrupting the turbulence convection considerably, and very possibly also affecting the turbulence production downstream. For $U_\infty = 10$, 12 and 15 m s^{-1}, the $\text{LEBU}_{2.5}$ entails $\tilde{h}u_\tau/\nu \approx 85$, 100 and 120, and $\tilde{h}/\delta_\circ \approx 0.22$, 0.23 and 0.24, respectively. This can be considered as a source targeting on the inner region of turbulent boundary layer at X_{ref}. Note that ν is the kinematic viscosity, and u_τ is the friction velocity determined from the measured baseline velocity profiles at X_{ref} by the Clauser method. On the other hand, $\text{LEBU}_{5.0}$ will double the values for both the $\tilde{h}u_\tau/\nu$ and $\tilde{h}/\delta_\circ$ above, resulting in a source targeting device that focuses on the outer region of the turbulent boundary layer at X_{ref}.

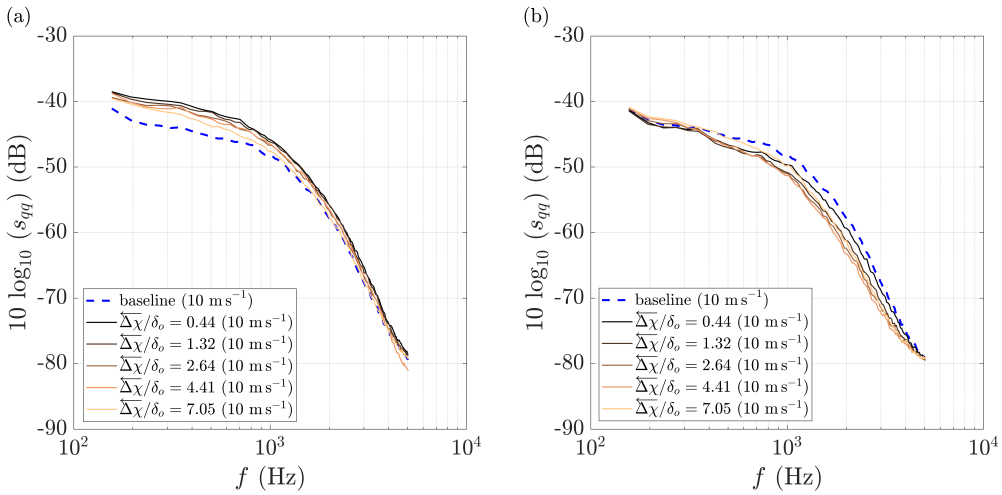

Fig. 6 Fluctuating wall pressure spectra s_{qq} at $\overrightarrow{\Delta x}/\delta_\circ = 3.52$ and $U_\infty = 10\ \text{m s}^{-1}$ for (a) $\text{LEBU}_{2.5}$, and (b) $\text{LEBU}_{5.0}$.

B. Wall pressure turbulence subjected to LEBU

The analysis will now focus on the power spectral density of the wall pressure fluctuations, s_{qq}. Under a combination of different $\overleftarrow{\Delta\chi}/\delta_\circ$, $\overrightarrow{\Delta x}/\delta_\circ$, $\tilde{h}$ and U_∞ in the test matrix, a very wide range of s_{qq} characteristics subjected to LEBU

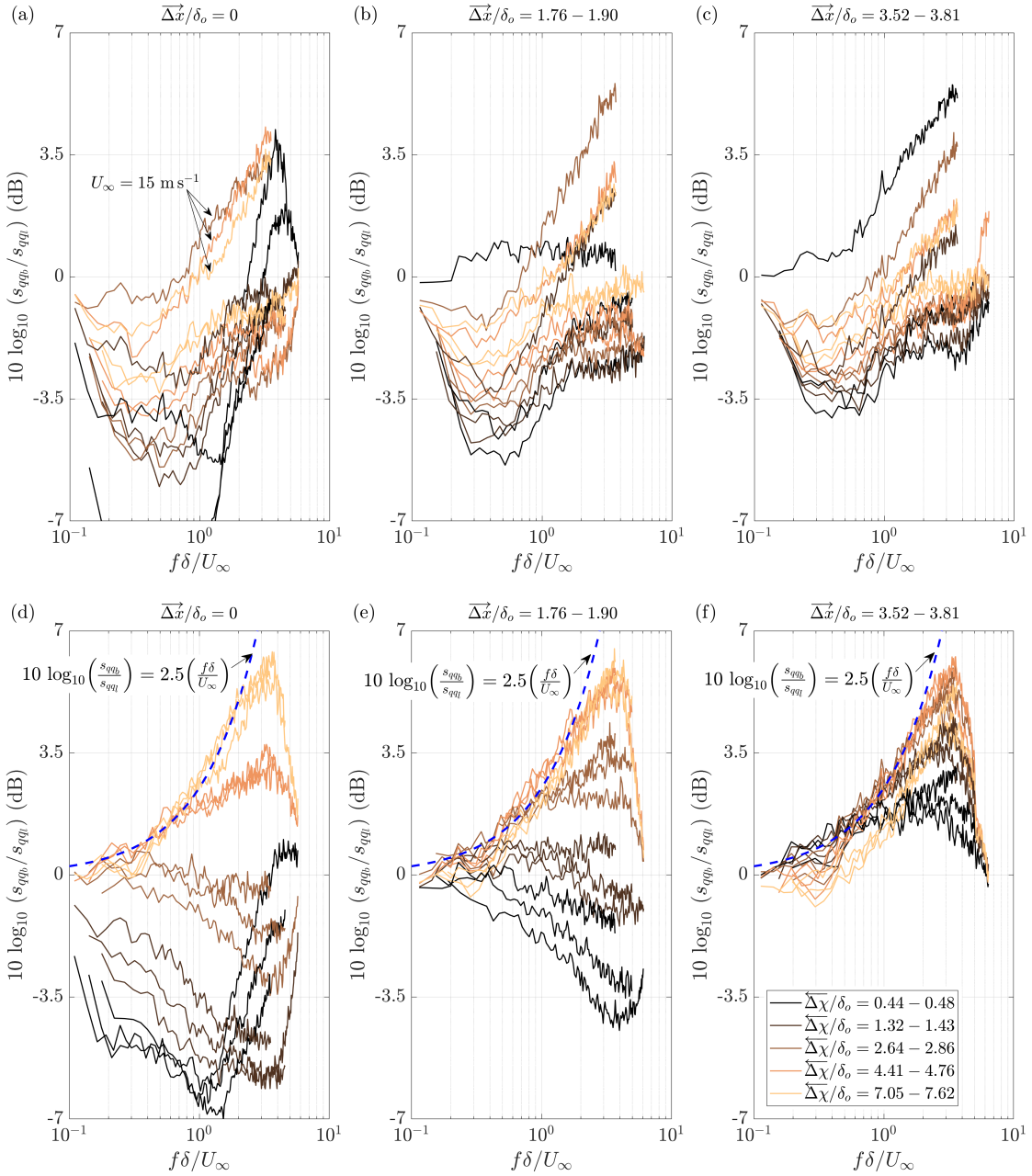

Fig. 7 Difference in the fluctuating wall pressure spectra between the baseline s_{qq_b} and those subjected to the LEBU s_{qq_l} measured across $0.44 \leq \overleftarrow{\Delta\chi}/\delta_\circ \leq 7.62$ for (a-c) LEBU$_{2.5}$, and (d-f) LEBU$_{5.0}$. Each sub-figure represents a collection of spectra pertaining to U_∞ = 10, 12 and 15 ms^{-1} at $\overrightarrow{\Delta x}/\delta_\circ$ = (a, d) 0, (b, e) $1.76 - 1.90$, and (c, f) $3.52 - 3.81$. The legends shown in sub-figure (f) is also applicable to other sub-figures.

has been observed. Figure 6 shows two examples of the s_{qq} spectra at $\overrightarrow{\Delta x}/\delta_\circ = 3.52$ and $U_\infty = 10$ ms^{-1} for both the LEBU$_{2.5}$ and LEBU$_{5.0}$. It is interesting to note that, despite the utilisation of the same LEBU under a same flow condition, placing it at different $\tilde{h}$ can produce significantly different unsteady wall pressure responses downstream.

To demonstrate all the results effectively, Figure 7 shows a summary of the difference in the fluctuating wall pressure spectra between the baseline, s_{qq_b} and those subjected to the LEBU, s_{qq_l}, which are measured across combination of $\overleftarrow{\Delta\chi}/\delta_\circ$, $\overrightarrow{\Delta x}/\delta_\circ$, $\tilde{h}$ and U_∞. The frequency is non-dimensionalised by the local boundary layer thickness δ corresponding to the individual $\overrightarrow{\Delta x}$ location, as well as the freestream velocity. A positive value of the $10\log_{10}(s_{qq_b}/s_{qq_l})$ denotes a reduction of wall pressure power spectral density level by the LEBU, and vice versa, when compared to the baseline level.

The analysis begins with Figure 7(a), which corresponds to the case of LEBU$_{2.5}$ and $\overrightarrow{\Delta x}/\delta_\circ = 0$ (i.e. X_{ref}). This sub-figure contains a collection of $10\log_{10}(s_{qq_b}/s_{qq_l})$ spectra pertaining to $U_\infty = 10$, 12 and 15 ms^{-1}. With the LEBU$_{2.5}$ placement at $0.44 \leq \overleftarrow{\Delta\chi}/\delta_\circ \leq 0.48$ (refer to sub-figure (f) for the legends), it is at a very close proximity to the surface microphone at $\overrightarrow{\Delta x}/\delta_\circ = 0$, which means that the latter is a direct recipient of the emanated near wake. The effect is clearly manifested in the production of significant negative values of $10\log_{10}(s_{qq_b}/s_{qq_l})$ across the low frequency range, reaching a negative trough (~ -10 dB) at $f\delta/U_\infty \approx 0.5$. However, as the frequency increases, the spectra undergoes a steep positive gradient, eventually reaching the positive territory of $10\log_{10}(s_{qq_b}/s_{qq_l})$ at the higher frequency range. This means that the turbulent boundary layer under this particular LEBU treatment has become highly non-equilibrium. At $U_\infty = 15$ ms^{-1}, there seems to be a deviation from the trend where the large scale turbulence structures at low frequency are perturbed less by the LEBU$_{2.5}$. At high frequency, the upstream placement of the LEBU$_{2.5}$ at $\overleftarrow{\Delta\chi}/\delta_\circ \geq 2.8$ can even achieve significant positive level of $10\log_{10}(s_{qq_b}/s_{qq_l})$ (> 3.5 dB), i.e. reduction in the wall pressure power spectral density level compared to the baseline counterpart. In other words, the seemingly under-performing LEBU$_{2.5}$ could improve when the freestream velocity increases at large $\overleftarrow{\Delta\chi}/\delta_\circ$. This might be due to the turbulent boundary layer becoming thinner at higher U_∞, causing the LEBU$_{2.5}$ to encounter larger effective $\tilde{h}^+$ locally. As a result, the LEBU$_{2.5}$ is increasingly situated near the outer layer. This highlights the importance to utilise LEBU effectively to target the large scale turbulence structures that are predominantly at the outer layer.

Within the same range of $\overleftarrow{\Delta\chi}/\delta_\circ$, it will be of interest to examine the effects of LEBU$_{2.5}$ to the fluctuating wall pressure at downstream locations. Figure 7(b) and 7(c) show the $10\log_{10}(s_{qq_b}/s_{qq_l})$ spectra at $\overrightarrow{\Delta x}/\delta_\circ = 1.76 - 1.90$, and $3.52 - 3.81$, respectively. At U_∞ =10 and 12 ms^{-1}, the trend of $10\log_{10}(s_{qq_b}/s_{qq_l})$ is still predominantly negative at the low frequency, but the level of negative will become less severe as the $\overrightarrow{\Delta x}/\delta_\circ$ increases. The same trend is also observed for the high frequency range where the magnitude of $10\log_{10}(s_{qq_b}/s_{qq_l})$ becomes closer to the zero datum, i.e. conforming to the baseline level. At $U_\infty = 15$ ms^{-1} and $\overrightarrow{\Delta x}/\delta_\circ = 1.76 - 1.90$, and $3.52 - 3.81$, the LEBU$_{2.5}$ follows the same trend at $\overrightarrow{\Delta x}/\delta_\circ = 0$ and continues to produce positive values of $10\log_{10}(s_{qq_b}/s_{qq_l})$ spectra at the mid and high frequencies.

Next, the $10\log_{10}(s_{qq_b}/s_{qq_l})$ spectra subjected to the LEBU$_{5.0}$ as a function of $\overleftarrow{\Delta\chi}/\delta_\circ$, $\overrightarrow{\Delta x}/\delta_\circ$ and U_∞ are shown in Figure 7(d−f). The LEBU$_{5.0}$ is found to be effective for the mitigation of wall pressure fluctuations. The following bullet points summarise the observations so far:

- if the trailing edge of the LEBU$_{5.0}$ is situated at exactly the same streamwise location as $\overrightarrow{\Delta x}/\delta_\circ = 0$, the corresponding vertical distance in wall unit is $\tilde{h}u_\tau/\nu \approx 170 - 240$ for the three freestream velocity cases. By traversing the LEBU$_{5.0}$ from $\overleftarrow{\Delta\chi}/\delta_\circ = 0.44$ to 7.62, the $\tilde{h}u_\tau/\nu$ will increase and be of higher values. This ensures that the LEBU$_{5.0}$ will always remain as a source targeting device for the outer part of turbulent boundary layer.
- not all position in $\overleftarrow{\Delta\chi}/\delta_\circ$ for the LEBU$_{5.0}$ will be effective for the mitigation of the wall pressure fluctuations. Based on the results in Figure 7(d−f), it is found that the $10\log_{10}(s_{qq_b}/s_{qq_l})$ will only become positive when $s' > 3$.
- the normalised frequency corresponding to the maximum wall pressure reduction always occurs at $f\delta/U_\infty = 3.5$.
- the variation in $10\log_{10}(s_{qq_b}/s_{qq_l})$ to the frequency is found to follow closely $2.5\left(f\delta/U_\infty\right)$, as shown in the figure. This represents the upper limit on the wall fluctuating pressure reductions by this particular type of LEBU.

After the discussion of the spectral characteristics, the overall wall pressure fluctuations S_{qq_l} subjected to the LEBU treatment can be examined. The S_{qq_l}, which is obtained by integrating the wall pressure fluctuation over a large frequency range $\int_f s_{qq_l} df$, can also be regarded as the standard deviation of the wall pressure fluctuations. Figure 8(a, b) show the variations of $10\log_{10}(S_{qq_b}/S_{qq_l})$ against s' at several targeting locations under a range of freestream

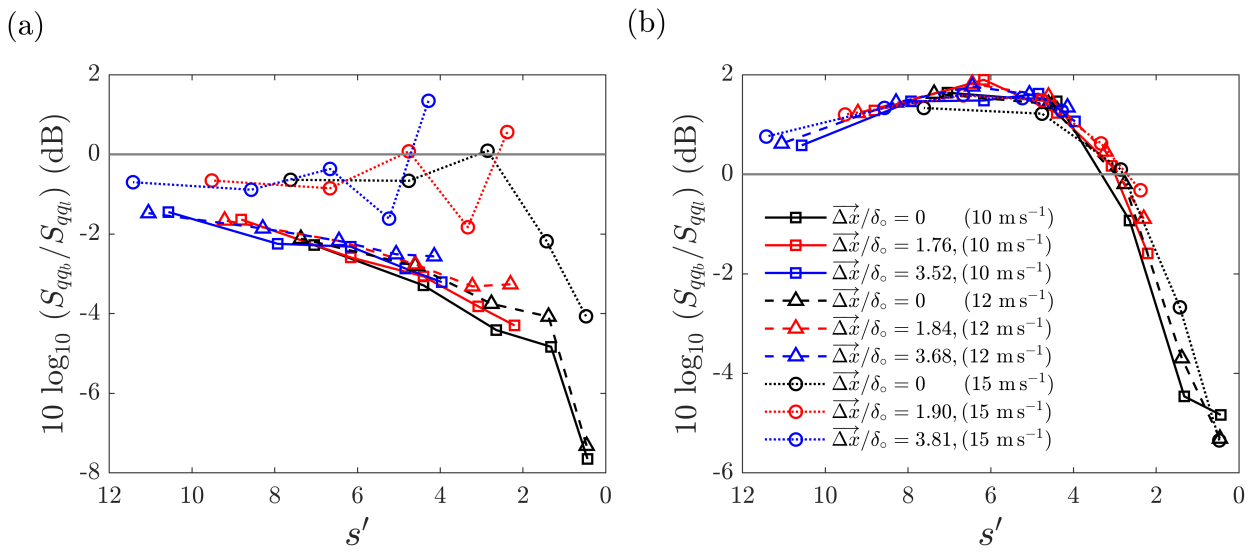

Fig. 8 Difference in the overall fluctuating wall pressure between the baseline S_{qq_b} and those subjected to the LEBU S_{qq_l} as a function of s' for (a) LEBU$_{2.5}$, and (b) LEBU$_{5.0}$. Each sub-figure represents a collection of overall values pertaining to U_∞ = 10, 12 and 15 ms^{-1} at $\overrightarrow{\Delta x}/\delta_\circ$ = 0, 1.76 − 1.90 and 3.52 − 3.81. The legend shown in sub-figure (b) is applicable to the sub-figure (a).

velocity. Note that the S_{qq_b} is the overall wall pressure fluctuations for the baseline case. Generally, the trends are very similar to the spectra discussed earlier. The inferiority of the LEBU$_{2.5}$ in mitigating the wall pressure fluctuation is again manifested in Figure 8(a) where negative values of $10\log_{10}(S_{qq_b}/S_{qq_l})$ are dominant. The curves collapse for both the U_∞ =10 and 12 ms^{-1} cases, where an initial detrimental outcome at low s' will gradually abate as the normalised separation distance between the LEBU and the targeting location increases. However, at U_∞ =15 ms^{-1}, where in previous analysis had indicated that the LEBU$_{2.5}$ is approaching the outer part of the turbulent boundary layer, deviation from the trend is obvious and the wall pressure fluctuations are now closer to the baseline levels.

An important outcome of this study is featured in Figure 8(b), where a high level of self-similarity behaviour is achieved by the LEBU$_{5.0}$ case throughout the ranges of normalised targeting location and freestream velocity investigated here. The onset of reduction for the overall wall pressure fluctuations is found to occur at $s' = 3$. The maximum reduction occurs at $s' = 6$. After that, the level of reduction will start to fall. Although the range of $\tilde{h}$ investigated here is not exhaustive, these non-dimensional values could represent a simple LEBU's optimisation rule in the mitigation of wall pressure fluctuations at zero pressure gradient flow.

C. Lateral turbulence length scales subjected to LEBU

The lateral (spanwise) coherence function of two microphone signals, γ_z^2, can describe a turbulence structure and its physical size in the frequency domain.

$$\gamma_z^2(f) = \frac{\left|\Phi_{z_i z_j}(f)\right|^2}{\Phi_{z_i z_i}(f)\,\Phi_{z_j z_j}(f)}. \tag{1}$$

In the equation, $\Phi_{z_i z_j}(f)$ is the cross power spectral density between two wall pressure fluctuating signals at locations z_i and z_j. The wall pressure signal at z_i is usually designated as the reference microphone sensor located at $\overrightarrow{\Delta x}/\delta_\circ = 0$ (X_{ref}), which is also at the mid-span ($z = 0$) of the flat plate. Therefore, $\Phi_{z_i z_i}(f)$ and $\Phi_{z_j z_j}(f)$ are the auto power spectral density for the reference (i) and j^{th} wall pressure fluctuations, respectively.

$$l_z(f) = \int_0^\infty \sqrt{\gamma_z^2(z,f)}\,\mathrm{d}z. \tag{2}$$

As shown in Equation 2, an integration of the spanwise coherence magnitude across the lateral location can result in

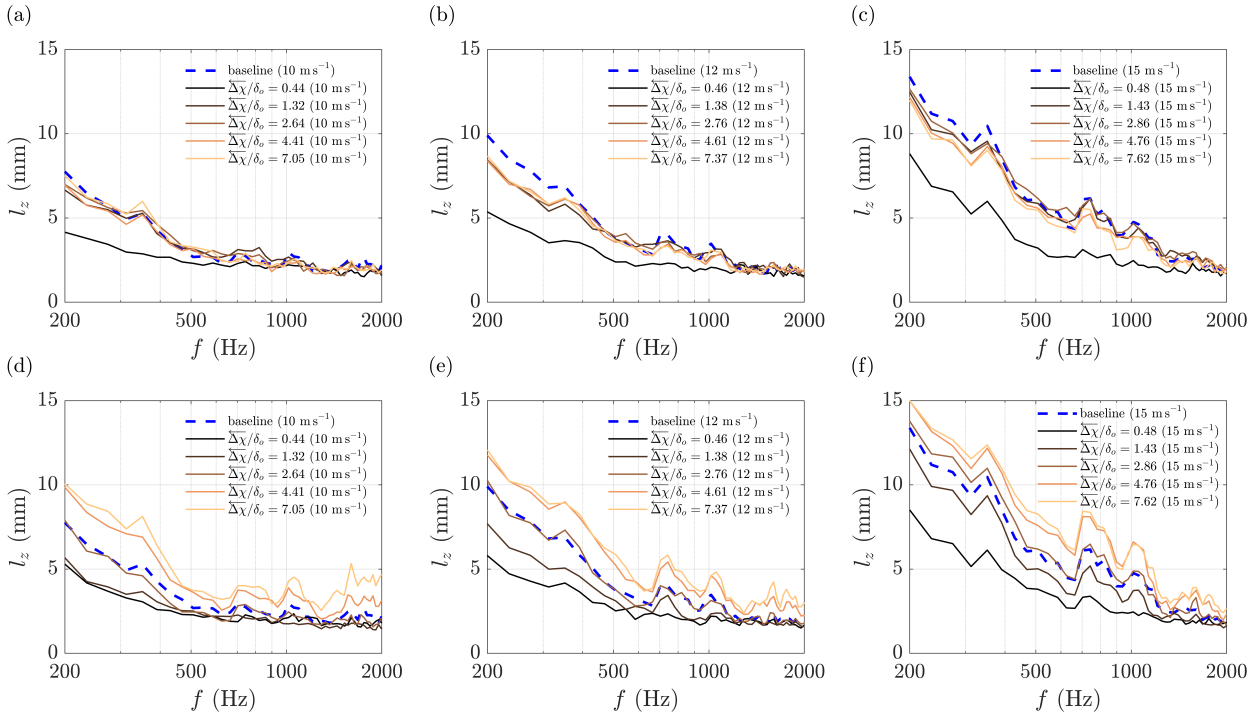

Fig. 9 Lateral coherence length spectra $l_z(f)$ at $\overrightarrow{\Delta x}/\delta_\circ = 0$ (X_{ref}), and U_∞ = (a, d) 10 ms^{-1}, (b, e) 12 ms^{-1} and (c, f) 15 ms^{-1} for (a–c) LEBU$_{2.5}$ and (d–f) LEBU$_{5.0}$. Each sub-figure contains the l_z spectra pertaining to the baseline and a range of $\overleftarrow{\Delta\chi}/\delta_\circ$.

the lateral coherence length of the turbulence, l_z, as a function of frequency. l_z is one of the important turbulent sources for the trailing edge noise radiation [8]. In the current work, a total of seven different Δz are used for the calculation of the l_z. This sub-section will study the responses of l_z subjected to both the LEBU$_{2.5}$ and LEBU$_{5.0}$ under different $\overleftarrow{\Delta\chi}/\delta_\circ$ and U_∞, but only at $\overrightarrow{\Delta x}/\delta_\circ = 0$ (X_{ref}). Therefore, from hereon, and also remainder of the paper, any expression of $\overleftarrow{\Delta\chi}/\delta_\circ$ is equivalent to s'.

Figure 9 shows the spectra of lateral coherence length l_z at $\overrightarrow{\Delta x}/\delta_\circ = 0$ for both the LEBU$_{2.5}$ and LEBU$_{5.0}$ at $10 \leq U_\infty \leq 15$ ms^{-1}. For the LEBU$_{2.5}$ case, there is a clear reduction of l_z when it is placed nearby the X_{ref} when $\overleftarrow{\Delta\chi}/\delta_\circ < 0.44 - 0.48$ against the baseline level. When the $\overleftarrow{\Delta\chi}/\delta_\circ$ increases, the differences in l_z against the baseline become smaller, but majority of them still exhibit lower levels. Therefore, as far as the lateral coherence length scale of the turbulence is concerned, the LEBU$_{2.5}$ is favourable for achieving low-noise aeroacoustics. Interestingly, this attribute would completely contradict to the responses in the wall pressure fluctuations where majority of them exhibit increase of magnitude against the baseline (see Figure 7a).

For the LEBU$_{5.0}$, placing it at close proximity to the X_{ref}, i.e. $\overleftarrow{\Delta\chi}/\delta_\circ < 0.44 - 0.48$ would repeat the previous trend where a significant reduction in the lateral coherence length is achieved across a large frequency range. However, at larger $\overleftarrow{\Delta\chi}/\delta_\circ$ distance, instead of conforming to the baseline level, the lateral coherence length continues to increase, even surpassing the baseline level when $\overleftarrow{\Delta\chi}/\delta_\circ > 3$. This attribute is again completely opposite to the wall pressure fluctuation counterparts, as shown in Figure 7(d).

D. Aeroacoustics properties subjected to (1) LEBU, and (2) RIBU

A trend now emerges that when a LEBU is placed at $s' < 3$, the intense interaction between the local turbulent boundary layer and the emanated near wake will enhance the wall pressure fluctuation, but weaken the lateral coherence length of the turbulence. The opposite can be said true, especially for the LEBU$_{5.0}$ case. When it is displaced further upstream from the targeted location, reduction of the wall pressure fluctuations against the baseline can be realised,

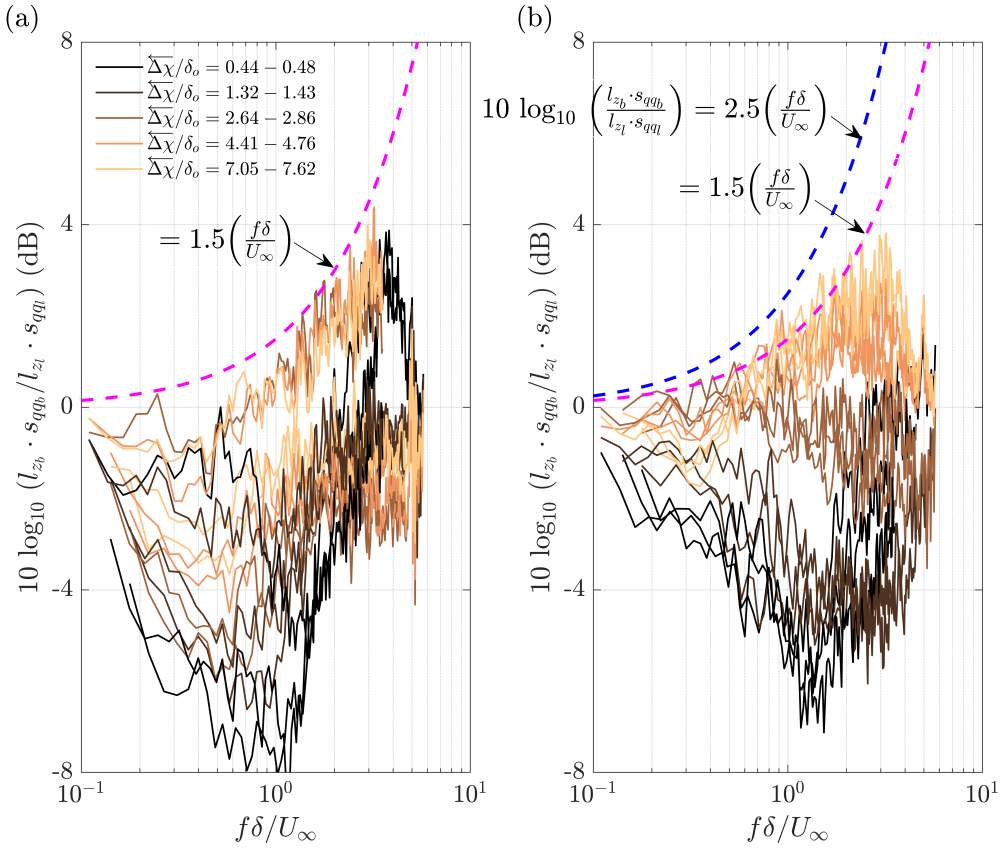

Fig. 10 Difference in the Amiet turbulent noise source between the baseline ($l_{z_b} \cdot s_{qqb}$) and those subjected to the LEBU ($l_{z_l} \cdot s_{qql}$) measured at $\overrightarrow{\Delta x}/\delta_\circ = 0$, i.e. at $X_{\mathbf{ref}}$, across a range of $\overleftarrow{\Delta X}/\delta_\circ$ for (a) $\mathbf{LEBU_{2.5}}$, and (b) $\mathbf{LEBU_{5.0}}$. Both sub-figures contain spectra measured at U_∞ = 10, 12 and 15 $\mathbf{ms^{-1}}$. Legends in sub-figure (a) are also applicable to (b).

but this comes at the expense of larger lateral coherence length of turbulence to be produced. How the aeroacoustics properties might be manipulated by these contradictory behaviours represent the focus of this section.

The relationship between the far field pressure (i.e. noise) and the near field wall pressure fluctuation near the trailing edge of an aerofoil is made explicitly in the classical work of [8], who derived a direct relationship between the power spectral density of the far field trailing edge noise (s_{pp}) of an aerofoil for an observer in the centre-line plane of an aerofoil with span $2d$, chord, $2b$, to the wall pressure spectra (s_{qq}) by:

$$s_{pp}(x, 0, y, \omega) = \left(\frac{\omega b y}{2\pi c_o \sigma^2}\right)^2 d|\mathfrak{L}|^2 \, l_z(\omega) s_{qq}(0, \omega), \tag{3}$$

where ω is the angular frequency, σ^2 is a Mach number corrected geometrical function, and $|\mathfrak{L}|$ is the norm of the acoustical transfer function. From Equation 3, the product of the lateral coherence length (l_z) and wall pressure spectra (s_{qq}) represents the main combined sources of the radiated spectrum (s_{pp}). Although no aeroacoustics measurement on aerofoil is performed in this study, it is still possible to evaluate the effect of LEBU on the trailing edge noise radiation by examining the $10\log_{10}(l_z \cdot s_{qq})$.

The results presented from hereon will only be based on the measurement conducted at $\overrightarrow{\Delta x}/\delta_\circ = 0$, i.e. X_{ref}. Figure 10(a−b) show the spectra of $10\log_{10}(l_{z_b} \cdot s_{qq_b}/l_{z_l} \cdot s_{qq_l})$, as a function of normalised frequency, for both the $\text{LEBU}_{2.5}$ and $\text{LEBU}_{5.0}$. The subscripts "b" and "l" represent the baseline and LEBU, respectively. A positive value denotes reduction of the Amiet noise sources against the baseline, and vice versa. The minima and maxima of the Amiet noise sources subjected to the $\text{LEBU}_{2.5}$ in Figure 10(a) largely occur at the same non-dimensional frequencies as the wall pressure fluctuations in Figure 7(a). However, the Amiet noise sources spectra would exhibit a better self-similarity behaviour than the wall pressure fluctuation spectra. In Figure 10(b) for the $\text{LEBU}_{5.0}$, the upper limit of the Amiet noise sources reduction is found to fit better to $1.5\big(f\delta/U_\infty\big)$, instead of the $2.5\big(f\delta/U_\infty\big)$ pertaining to the upper limit for the wall pressure fluctuations as depicted in Figure 7(d−f). This phenomenon is a manifestation of the counter-balancing effect between the wall pressure fluctuation and turbulence lateral coherence length.

Although the $\text{LEBU}_{2.5}$ is not as effective as the $\text{LEBU}_{5.0}$ in the suppression of the Amiet noise sources, a number of common characteristics can still be extracted from Figure 10(a−b). First, the minima and maxima of the $10\log_{10}(l_{z_b} \cdot s_{qq_b}/l_{z_l} \cdot s_{qq_l})$ occur at $f\delta/U_\infty \approx 1$ and 3.5, respectively. Second, the upper limit of the Amiet noise sources reduction, $1.5\big(f\delta/U_\infty\big)$, is applicable to both cases. Third, reduction of the Amiet noise sources is not possible at the low frequency, typically at $f\delta/U_\infty < 0.3$. This represents the limitation of LEBU in tackling the low frequency noise source.

Using the same experimental setup and analysis techniques as the current one, we have observed that targeting the near wall turbulence by the riblets can reduce the Amiet noise sources at low and high frequencies, but exhibit no effect at the mid frequency region [2]. The different sensitivity responses of the Amiet noise sources against the riblets and LEBU, respectively, raise a research question of whether they can complement each other to destroy the Amiet noise sources. Although a comprehensive investigation of this research topic is beyond the current scope, some preliminary investigations of the RIBU have been conducted and the results are presented here.

Using the exact same LEBU configurations and $\overleftarrow{\Delta\chi}/\delta_\circ$ range that produced Figure 10(a−b), but with the addition of riblets whose configuration is shown in Figure 3, Figure 11(a−b) shows the $10\log_{10}(l_{z_b} \cdot s_{qq_b}/l_{z_r} \cdot s_{qq_r})$ spectra for the RIBU cases. Note that l_{z_r} and s_{qq_r} are the spanwise turbulence coherence length and wall pressure fluctuations, respectively, subjected to the RIBU treatment. The coverage of the riblets starts at $\overrightarrow{\Delta x}/\delta_\circ = -11.5$, and ends at $\overrightarrow{\Delta x}/\delta_\circ = 11.5$. This means that the riblets will coincide with the entire LEBU locations of $0.44 \leq \overleftarrow{\Delta\chi}/\delta_\circ \leq 7.62$. The followings summarise five major characteristics of the RIBU, which can be cross-referenced to the annotations in the figure:

(A) The abilities of the riblets to reduce both the spanwise turbulence coherence length and wall pressure fluctuations at low frequency, which have been demonstrated in [2], seem to transfer to the RIBU whereby the enhancement of the Amiet noise sources at low frequency by the $\text{LEBU}_{2.5}$ (see Figure 10a) can be mitigated by the addition of the riblets. The minima of the $10\log_{10}(l_{z_b} \cdot s_{qq_b}/l_{z_r} \cdot s_{qq_r})$ also appear to be shifted from $f\delta/U_\infty = 1$ to $f\delta/U_\infty = 0.6$.

(B) The addition of riblets in conjunction with the $\text{LEBU}_{2.5}$ has a significant impact on the maxima of $10\log_{10}(l_{z_b} \cdot s_{qq_b}/l_{z_r} \cdot s_{qq_r})$. First, the level of the maxima has increased from 4 dB to 6 dB. Second, a clear trend has been established that the RIBU is the most effective at the lowest $\overleftarrow{\Delta\chi}/\delta_\circ$, and deteriorates as the $\overleftarrow{\Delta\chi}/\delta_\circ$ increases. Third, the maxima frequency appears to remain unchanged at $f\delta/U_\infty = 3.5$. The upper limit of the Amiet noise

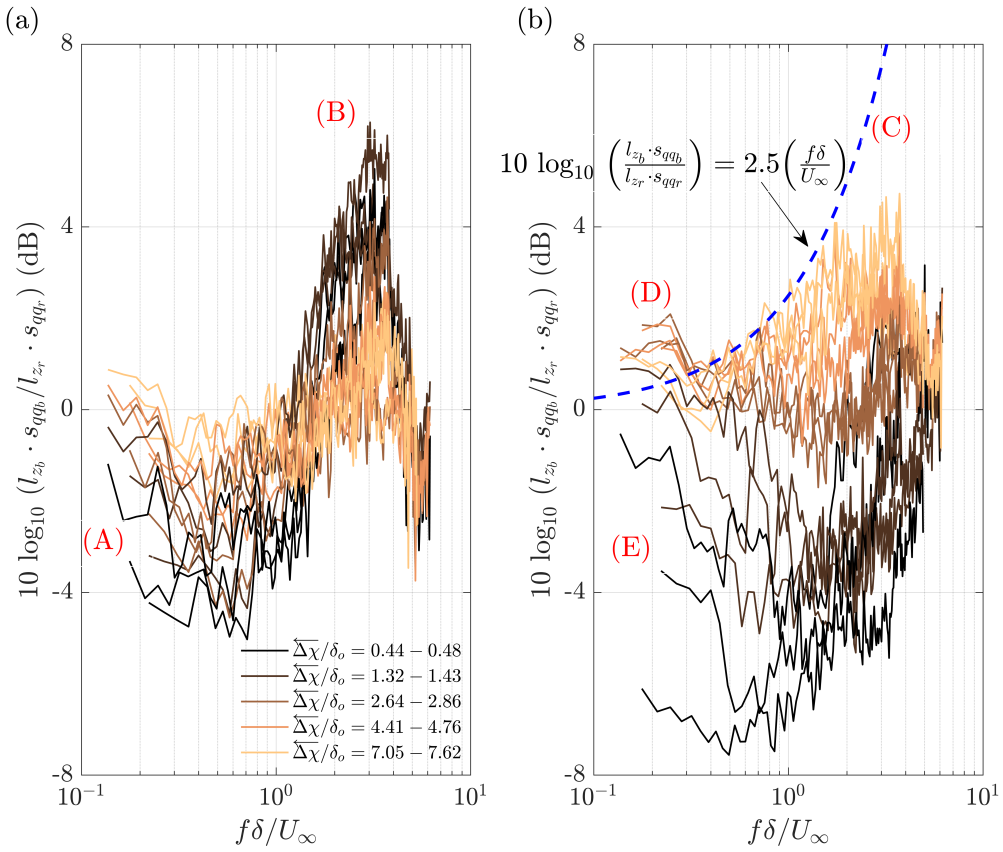

Fig. 11 Difference in the Amiet turbulent noise sources between the baseline ($l_{z_b} \cdot s_{qqb}$) and those subjected to the RIBU ($l_{z_r} \cdot s_{qqr}$), where RIBU = riblets+LEBU. The results are measured at $\overrightarrow{\Delta x}/\delta_\circ = 0$, i.e. at $X_{\mathbf{ref}}$, across a range of $\overleftarrow{\Delta\chi}/\delta_\circ$ for (a) riblets+LEBU$_{2.5}$, and (b) riblets+LEBU$_{5.0}$. Both sub-figures contain spectra measured at U_∞ = 10, 12 and 15 ms^{-1}. Legends in the sub-figure (a) are also applicable to (b).

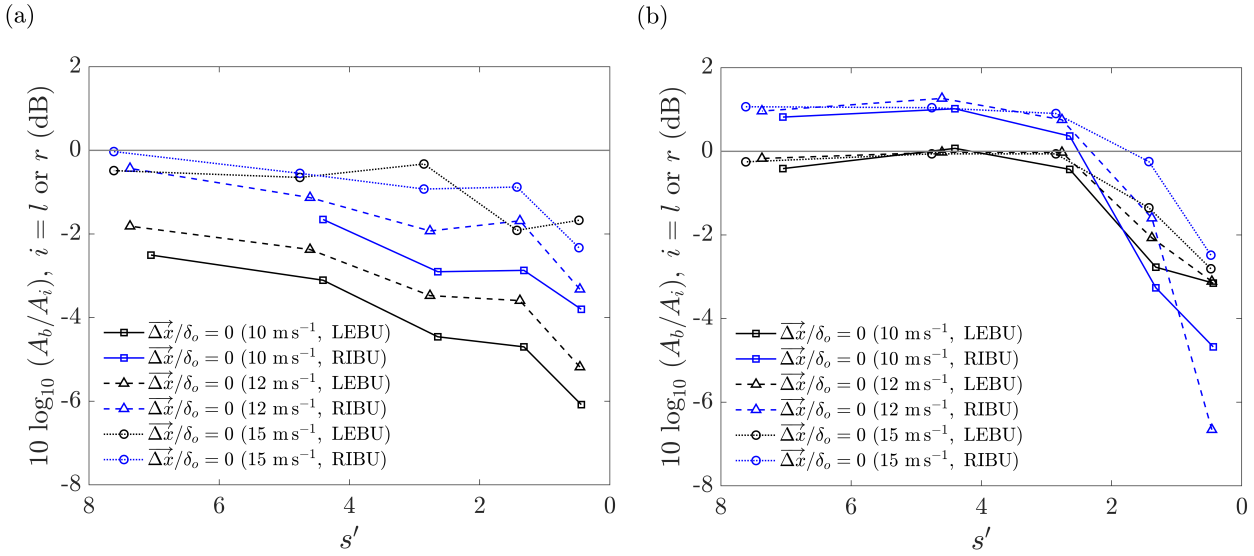

Fig. 12 Difference in the overall Amiet noise sources between the baseline $l_{z_b} \cdot s_{qq_b}$ and those subjected to the RIBU $l_{z_r} \cdot s_{qq_r}$ measured at $\overrightarrow{\Delta x}/\delta_\circ = 0$, i.e. at X_{ref}, across a range of s' $(= \overleftarrow{\Delta\chi}/\delta_\circ + 0)$ for (a) LEBU$_{2.5}$ and riblets, and (b) LEBU$_{5.0}$ and riblets. Both sub-figures contain the overall values measured at U_∞ = 10, 12 and 15 ms^{-1}.

sources reduction also becomes a function of the logarithmic, instead of behaving linearly, against the frequency, i.e. the curves do not follow the $1.5(f\delta/U_\infty)$ anymore.

(C) The addition of riblets in conjunction with the LEBU$_{5.0}$ can revert the upper limit of the Amiet noise sources reduction back to the $2.5\big(f\delta/U_\infty\big)$, which is an improvement over the LEBU-only case.

(D) More significantly, the ability to reduce the Amiet noise sources at low frequency by the riblets has been successfully replicated in the RIBU configuration where up to 2 dB can be harnessed when $\overleftarrow{\Delta\chi}/\delta_\circ \geq 2.64$.

(E) At $\overleftarrow{\Delta\chi}/\delta_\circ < 2.64$, however, the addition of riblets seems to be a disadvantage where the otherwise self-similar behaviour is destroyed, and in some cases, a significant enhancement of the Amiet noise sources can be resulted.

Generally, the RIBU can improve the self-similar behaviour of the Amiet noise sources spectra, except for the situation in (E) as described above. The RIBU can also enhance the maxima of the Amiet noise sources reduction (B), and most importantly, it has a potential to achieve an enhanced noise reduction across a very large range of frequency as demonstrated in (C) and (D).

The performance of the LEBU and RIBU can also be examined in the context of frequency-integrated Amiet noise sources:

$$A_i = \int_f \Big[l_{z_i}(f) \cdot s_{qq_i}(f) \Big] df, \quad i = b,\ l \text{ or } r, \tag{4}$$

where b, l and r refer to the baseline, LEBU and RIBU, respectively. Hence, the overall performance of the LEBU and RIBU against s' $(= \overleftarrow{\Delta\chi}/\delta_\circ{+}0)$ can be quantified in the expression of $10\log_{10}(A_b/A_l)$ and $10\log_{10}(A_b/A_r)$, as shown in Figure 12.

In Figure 12(a), the trend of a slow recovery towards the baseline level for the overall Amiet noise sources, as s' increases, is similar to the overall wall pressure fluctuations in Figure 8(a). The RIBU consistently outperforms the LEBU counterparts, except at U_∞ = 15 ms^{-1} where the differences become smaller. In some cases, the LEBU is better than the RIBU. As reported in [2], the capability of the riblets to reduce high frequency Amiet noise sources weakens as the freestream velocity increases. Owing to the thinning of the turbulent boundary layer thickness, the riblets are increasingly behaving as a surface roughness, which is expected to exacerbate the LEBU at $\tilde{h}$ = 2.5 mm whose emanated wake will be close to the wall surface. The combination of these will increase the level of wall pressure fluctuation instead of reducing it. Nevertheless, there is no evidence that the Amiet noise sources can be reduced by either the LEBU or RIBU in configurations that cause the outcomes in Figure 12(a).

At $\tilde{h}$ = 5.0 mm for the LEBU, however, the addition of riblets can exert a great impact to the reduction of overall

Amiet noise sources, as shown in Figure 12(b). Both the LEBU and RIBU exhibit good self-similarity behaviours, respectively. While the LEBU alone can only just manage to match the same level of the overall Amiet noise sources against the baseline case (due to the counter-balancing of the s_{qq_i} and l_{z_i}), the RIBU is shown to be capable of achieving an overall reduction of up to 1.5 dB at $s' > 3$.

The RIBU can potentially be an effective source targeting device to mitigate the turbulent noise sources, and achieve self-noise reduction. It is hoped that the preliminary results presented here can attract attentions in future research to understand the physical mechanisms and exploit the benefits.

IV. Conclusion

A successful mitigation of the Amiet's turbulent noise sources should be underpinned by reductions in both the wall pressure fluctuation and lateral coherence length scale. The Large Eddy BreakUp (LEBU) device, if placed strategically at the outer part of a turbulent boundary layer, and $s' > 3$, would be able to achieve reductions of the wall pressure fluctuations especially at the mid and high frequency ranges. However, what appears to be the optimal LEBU configuration for the mitigation of wall pressure fluctuation will not be reciprocated in the lateral coherence length, where an increase across a large range of frequency has been observed when $s' > 3$.

While the wall pressure fluctuations is insensitive to the LEBU at low frequency, the lateral coherence length scale at low frequency can even be enhanced if the LEBU is placed at $s' > 3$. When the Amiet noise source spectrum is integrated across the frequency to obtain the overall level, contribution from the low frequency component will be the most dominant. Therefore, using the LEBU alone is unable to reduce the overall, frequency-integrated Amiet noise source.

In our previous study, riblets as a near wall device have been found to reduce both the wall pressure fluctuations and lateral coherence length scales at low frequency. When the riblets and LEBU are used concurrently (RIBU), they can target the turbulent boundary layer independently without much interference against each other. Indeed, the low frequency component of the Amiet turbulent noise sources can be reduced by the RIBU. In addition, reduction of the mid frequency component is further enhanced. Hence, using the RIBU can reduce the frequency-integrated, overall Amiet noise source, and potentially, the trailing edge noise.

Acknowledgments

The authors would like to thank the PhD studentship sponsored by the Thomas Gerald Gray Charitable Trust in the United Kingdom.

References

[1] Brooks, T. F., Pope, S. D., and Marcolini, M. A., "Airfoil self-noise and prediction," NASA Reference Publication 1218, Retrieved from: https://ntrs.nasa.gov/archive/nasa/casi.ntrs.nasa.gov/19890016302.pdf, NASA Langley Research Center, Hampton (VA), 1989. (Accessed: 2020-04-08).

[2] Muhammad, C., and Chong, T. P., "Mitigation of turbulent noise sources by riblets," *Journal of Sound and Vibration*, Vol. 541, 2022, p. 117302. https://doi.org/https://doi.org/10.1016/j.jsv.2022.117302.

[3] Yajnik, K. S., and Acharya, M., "Non-equilibrium effects in a turbulent boundary layer due to the destruction of large eddies," *Structure and Mechanisms of Turbulence I*, edited by H. Fiedler, Springer Berlin Heidelberg, Berlin, Heidelberg, 1978, pp. 249–260. https://doi.org/10.1007/3-540-08765-6_24.

[4] Hefner, J. N., Weinstein, L. M., and Bushnell, D. M., *Large-Eddy Breakup scheme for turbulent viscous drag reduction*, 1980, pp. 110–127. https://doi.org/10.2514/5.9781600865466.0110.0127.

[5] Savill, A. M., and Mumford, J. C., "Manipulation of turbulent boundary layers by outer-layer devices: skin-friction and flow-visualization results," *Journal of Fluid Mechanics*, Vol. 191, 1988, p. 389–418. https://doi.org/10.1017/S0022112088001624.

[6] Gruber, M., "Airfoil noise reduction by edge treatments," *PhD Thesis, University of Southampton.* , 2012. https://doi.org/http://eprints.soton.ac.uk/id/eprint/349012.

[7] Garcia Sagrado, A. P., "Boundary layer and trailing edge noise sources," Ph.D. thesis, University of Cambridge, 2008.

[8] Amiet, R. K., "Noise due to turbulent flow past a trailing edge," *J. Sound. Vib.*, Vol. 47, 1976, pp. 387–393. https://doi.org/10.1016/0022-460X(76)90948-2.